



## A Measurement of the Forward-Backward Asymmetry in the Production of $B^\pm$ Mesons in $p\bar{p}$ Collisions

The DØ Collaboration  
URL <http://www-d0.fnal.gov>  
(Dated: July 14, 2014)

We present a preliminary measurement of the forward-backward asymmetry in the production of  $B^\pm$  mesons,  $A_{FB}(B^\pm)$ , using  $B^\pm \rightarrow J/\psi K^\pm$  decays in  $10.4 \text{ fb}^{-1}$  of  $p\bar{p}$  collision data from Run II of the DØ Experiment at the Tevatron Collider. A non-zero asymmetry would indicate a preference for a particular flavor of  $b$  quark to be produced in the direction of the proton beam.  $A_{FB}(B^\pm)$  is extracted from a maximum likelihood fit to the difference between forward- and backward-produced  $B^\pm$  mesons, using a boosted decision tree to reduce background. Corrections are made for reconstruction asymmetries of the decay products. We measure  $A_{FB}(B^\pm) = [-0.26 \pm 0.41 \text{ (stat.)} \pm 0.17 \text{ (syst.)}]%$  which is consistent with zero. Standard Model predictions based on next-to-leading-order Monte Carlo calculations are in preparation.

*Preliminary Results for Summer 2014 Conferences*

## I. INTRODUCTION

A forward-backward asymmetry in the production of heavy quarks can be caused by interference between next-to-leading order processes, such as gluon radiation in  $q\bar{q}$  interactions and  $qg$  scattering [1]. Examples of interfering diagrams are shown in Fig. 1. Over the past few years, there has been a great deal of interest in the the forward-backward asymmetry in  $t\bar{t}$  production ( $A_{FB}^{t\bar{t}}$ ) [2], especially since experimental results have been reported to be larger than standard model predictions [3, 4]. The most recent  $D\bar{O}$  measurements agree with the standard model [5], as do measurements at the LHC, where asymmetries are expected to be smaller since  $t\bar{t}$  production is dominated by gluon-gluon fusion [6, 7]. Large  $t\bar{t}$  production asymmetries at the Tevatron prompted development of models which could explain the excess.  $A_{FB}^{b\bar{b}}$  has the same source as  $A_{FB}^{t\bar{t}}$  but is expected to have a smaller magnitude in the standard model, making it an important probe of these new physics models [8].  $A_{FB}^{b\bar{b}}$  in  $b$ -jets has only recently been measured at hadron collider experiments [9, 10]. These measurements are impacted by the need to correctly identify the initial quark content of  $b$  jets and their flavor ( $b$  or  $\bar{b}$ ).

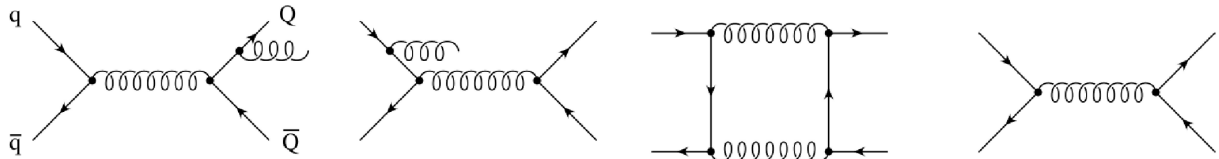


FIG. 1: Next-to-leading order diagrams which lead to a forward-backward asymmetry in heavy quark production through interference.

At  $D\bar{O}$  we have chosen to use fully-reconstructed  $B^\pm \rightarrow J/\psi K^\pm$  decays, since reconstructing a  $B^\pm$  allows for direct quark flavor identification with no need to account for mixing and no ambiguity in quark flavor. We define a forward-backward asymmetry as  $A_{FB} = (N_F - N_B)/(N_F + N_B)$ . In  $p\bar{p}$  collisions, the forward category indicates a quark (or  $B^-$  meson) with the longitudinal component of its momentum in the direction of the proton beam, or an anti-quark (or  $B^+$  meson) with the longitudinal component of its momentum in the direction of the anti-proton beam.

In each event we reconstruct a  $B^\pm$  meson from one of the quarks and categorize it as forward or backward with a “charge”  $q_{FB} = -q_B \text{sgn}(\eta_B)$ , where  $\text{sgn}(x)$  is the sign function and  $\eta_B$  is the pseudorapidity of the  $B^\pm$ ,  $\eta = -\frac{1}{2} \ln[\tan(\theta/2)]$ . Figure 2 gives examples of the forward and backward categories. The forward-backward asymmetry of the  $B^\pm$  mesons is:

$$A_{FB}(B^\pm) = \frac{N(-q_B\eta_B > 0) - N(-q_B\eta_B < 0)}{N(-q_B\eta_B > 0) + N(-q_B\eta_B < 0)}. \quad (1)$$

## II. THE $D\bar{O}$ DETECTOR

The  $D\bar{O}$  experiment collected data at the Fermilab Tevatron  $p\bar{p}$  Collider at  $\sqrt{s} = 1.96$  TeV from 2001 through the shutdown of the Tevatron in 2011, a period referred to as Run II. The  $D\bar{O}$  detector is described in detail elsewhere [11]. For the purposes of this analysis, the most important parts of the detector are the central tracker and the muon system.

The inner region of the  $D\bar{O}$  central tracker consists of a silicon microstrip tracker (SMT) that covers pseudorapidities  $|\eta| < 3$ . In the spring of 2006, an additional layer of silicon (Layer 0) was added close to the beam pipe [12]. Since the detector configuration changed significantly with this addition, the  $D\bar{O}$  dataset is divided into two distinct periods, Run IIa and Run IIb, with the analysis performed separately for each period. Run IIb is further divided into subsets referred to as Run IIb1 – Run IIb4, with each period separated by several-week-long accelerator shut-downs.

Moving away from the interaction region, the next detector subsystem encountered is the  $D\bar{O}$  central fiber tracker (CFT), which consists of 16 concentric cylinders of scintillating fibers, covering  $|\eta| < 2.5$ . Both the SMT and CFT are located within a 2 T superconducting solenoidal magnet. The  $D\bar{O}$  muon system is located outside of the finely segmented liquid argon sampling calorimeter.

The muon system consists of three layers of tracking detectors and trigger scintillators, one layer in front of 1.8 T toroidal magnets and two additional layers after the toroids. The muon system has a large acceptance, with coverage for  $|\eta| < 2$ . The muon system has minimal background from hadron punch-through, providing efficient reconstruction of  $J/\psi \rightarrow \mu^+\mu^-$  decays. Also, the regular reversal of solenoid and toroid magnet polarities allows for the cancellation

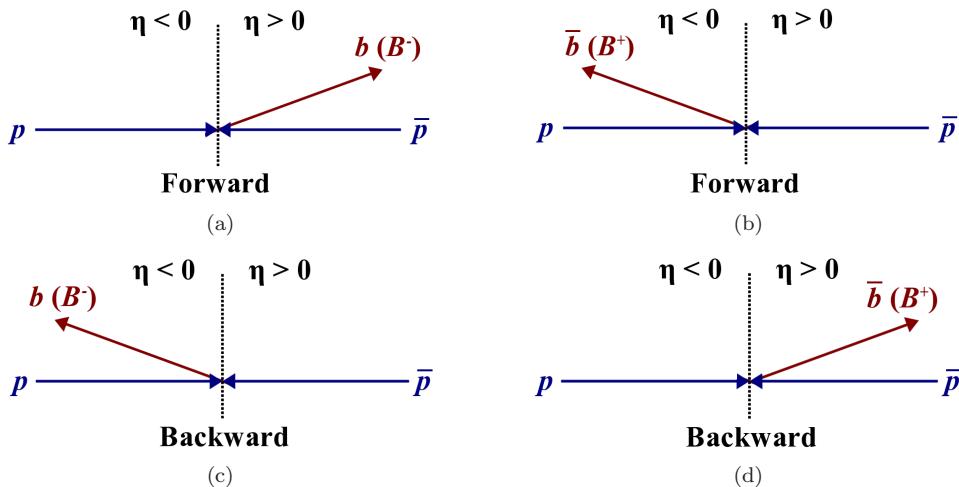


FIG. 2: Diagrams illustrating the definitions of (a,b) forward particles with  $q_{FB} = +1$  and (c,d) backward particles with  $q_{FB} = -1$ .

of first-order detector-based asymmetries. The data used in this analysis were collected with a suite of single muon and dimuon triggers.

### III. THEORETICAL PREDICTIONS

Until lately, theoretical predictions of  $A_{FB}^{b\bar{b}}$  were limited [1]. Based on the plethora of  $t\bar{t}$  asymmetry measurements in recent years, new predictions for heavy-flavor production asymmetries have been published comparing the Standard Model with new physics models. Inclusive predictions for  $A_{FB}^{b\bar{b}}$  are on the order of 0.5% [8, 13], but the mass scales of the  $b\bar{b}$  pairs considered are better suited to a jet-based analysis.

To make Standard Model predictions tailored to the kinematics and selections of this analysis, we produce next-to-leading-order Monte Carlo (MC) samples for the process  $p\bar{p} \rightarrow b\bar{b}X$ . Monte Carlo events are produced using MC@NLO for event generation, with parton distribution function set CTEQ6M1, and HERWIG for parton showering and hadronization [14–16]. Detector simulation was done using GEANT3 [17]. This prediction is in preparation; the systematic uncertainties due to scale, fragmentation, and other effects need to be determined.

Because the definitions of forward and backward are tied directly to  $\text{sgn}(\eta_B)$ , the ambiguous region near  $\eta_B = 0$  must be considered. A resolution study of  $\eta_B$  at production and reconstruction shows that rejecting events with  $|\eta_B| < 0.1$  removes the ambiguity to a high degree, as shown in Fig. 3(a). This cut removes approximately 2% of the data sample and has a negligible effect on the measured value of  $A_{FB}(B^\pm)$ . The difference between the direction of the reconstructed  $B^\pm$  and the initial  $b$  quark is shown in Fig. 3(b). In approximately 80% of events the value of  $q_{FB}$  for the  $B^\pm$  matches  $q_{FB}$  for the quark.

### IV. EVENT SELECTION AND MONTE CARLO

Events containing  $B^\pm \rightarrow J/\psi K^\pm$  candidates are selected from the full DØ Run II dataset. Candidates are reconstructed by identifying a pair of oppositely-charged muons (decay products of the  $J/\psi$  particle) that are produced along with a charged track at a common vertex. Displacement of this vertex from the primary beam interaction vertex due to the decay length of the weakly decaying  $B$  mesons is essential for identifying  $B^\pm$  candidates.

All particles are required to lie within the pseudorapidity coverage of the muon and central tracking systems,  $|\eta| < 2.1$ . Muons must have a minimum transverse momentum of 1.5 GeV/ $c$ , and the  $K^\pm$  candidate must have a minimum  $p_T$  of 0.7 GeV/ $c$ . All three tracks must have at least two hits in both the silicon microstrip and central fiber trackers. One muon must have hits in both inner and outer layers of the muon detector, and the other muon must hit at least one layer. Both tracks in the muon system must match to tracks in the central tracking system [18].

$J/\psi$  candidates with reconstructed invariant mass between 2.7 and 3.45 GeV/ $c^2$  are accepted, and the uncertainty on the particle’s decay length must be less than 0.1 cm. The cosine of the  $J/\psi$ ’s two-dimensional “pointing angle” (the angle between the vector from the primary vertex to the  $J/\psi$  vertex and the dimuon momentum vector) is required

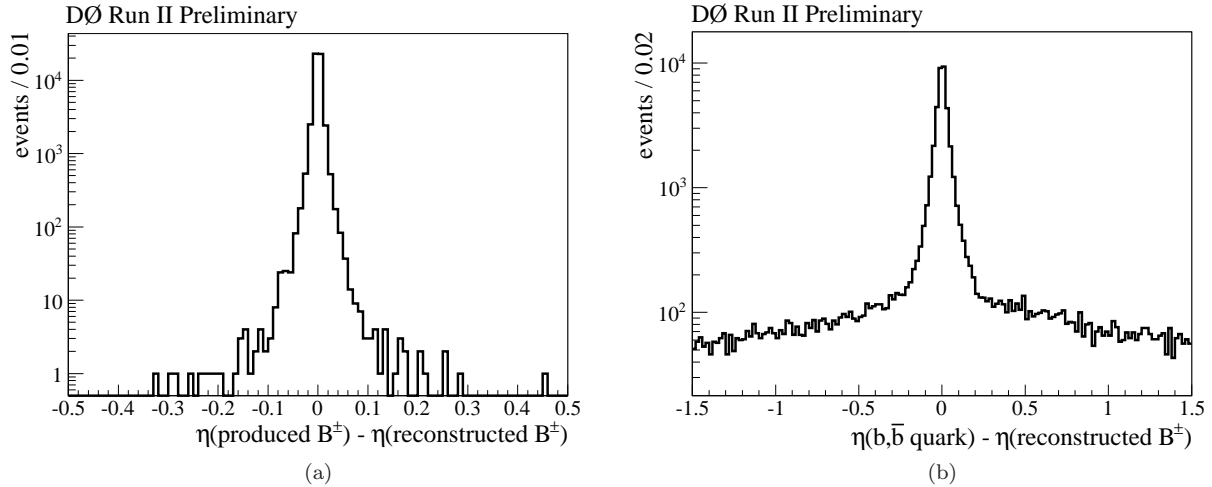


FIG. 3: (a)  $\eta_B(\text{produced}) - \eta_B(\text{reconstructed})$  for MC@NLO  $B^\pm$  candidates. Events with  $|\eta_B| < 0.1$  are rejected. (b)  $\eta(\text{quark}) - \eta_B(\text{reconstructed})$  in MC@NLO, showing the relationship between the direction of the  $b$  quark and the reconstructed  $B^\pm$  meson.

to be greater than zero. We correct the muon momenta to constrain the  $\mu^+\mu^-$  invariant mass to the world average of the  $J/\psi$  mass in the calculation of the  $B^\pm$  candidate mass [19].

$B^\pm$  candidates are accepted if their transverse decay length significance (defined as the transverse decay length divided by its uncertainty) is greater than 3.0. The reconstructed  $\mu^+\mu^-K^\pm$  vertex must have goodness-of-fit quantity  $\chi^2 < 16$ , and the cosine of the  $B^\pm$  pointing angle is required to be above 0.8. The selected  $B^\pm$  mass range for this analysis is  $5.05 - 5.65 \text{ GeV}/c^2$ .

Background rejection is achieved using a boosted decision tree (BDT) trained on simulated signal from Monte Carlo and background events from  $B^\pm$  sidebands above and below the selected mass range ( $4.0 - 5.05$  and  $5.65 - 7.0 \text{ GeV}/c^2$ ) [20]. Leading-order  $B^\pm \rightarrow J/\psi K^\pm$  MC events generated with PYTHIA are processed through the same reconstruction code as used for data [21]. The Monte Carlo events are weighted to give optimal agreement between data and simulation. The muon trigger efficiency in particular is not modeled during MC generation, so the transverse momenta of both muons must be reweighted. A cut on the BDT discriminant of  $-0.002$  is chosen to minimize the uncertainty of  $A_{FB}(B^\pm)$ . Figure 4 shows the uncertainty in  $A_{FB}(B^\pm)$  and the signal significance as a function of BDT discriminant.

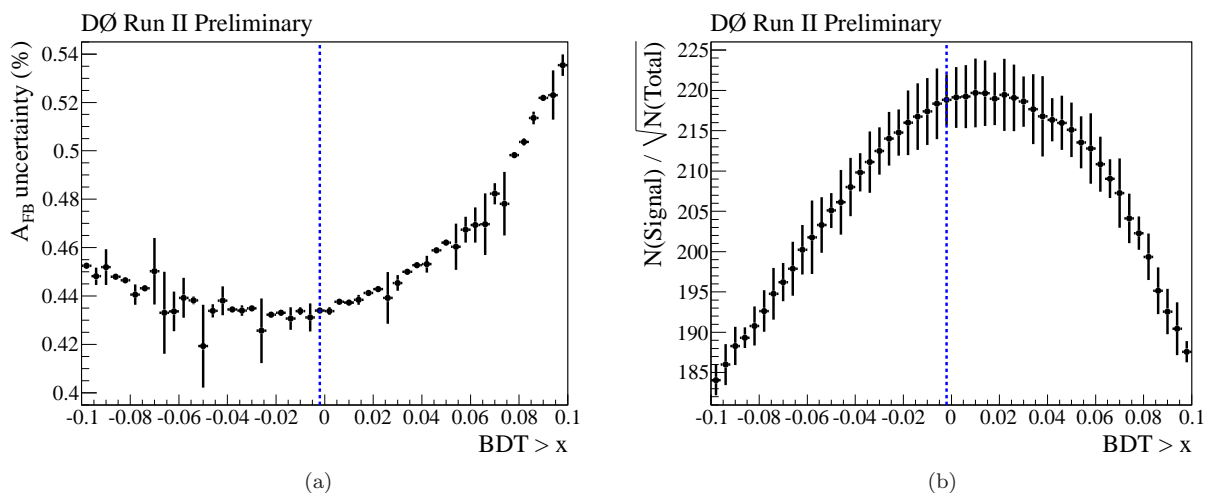


FIG. 4: The BDT minimum value of  $-0.002$  was chosen to (a) minimize the uncertainty on  $A_{FB}$  and (b) provide a large signal fraction in the final data sample. Errors represent the combination of five trials each with a different random seed to blind  $q_{FB}$  (see Sec. VII).

## V. MAXIMUM LOG LIKELIHOOD FIT

A maximum log likelihood fit incorporating a signal probability distribution function (PDF) and three background PDFs is used to extract  $A_{FB}(B^\pm)$ . The PDFs are functions of the candidate  $B^\pm$  mass  $m_{J/\psi K}$  and the kaon energy  $E_K$ . The signal PDF  $S(m_{J/\psi K}, E_K)$  is modeled as a normalized double Gaussian function where both Gaussians have the same mean ( $m_B$ ) but different widths ( $\sigma_{\text{outer}}, \sigma_{\text{inner}}$ ). The fraction of the inner Gaussian is labeled  $f$ , and both widths vary with  $E_K$ . The form of the dependence was determined empirically by fitting in bins of  $E_K$ ,

$$S(m_{J/\psi K}, E_K) = \frac{1-f}{\sigma_{\text{outer}}\sqrt{2\pi}} \exp\left(\frac{-(m_{J/\psi K} - m_B)^2}{2\sigma_{\text{outer}}^2}\right) + \frac{f}{\sigma_{\text{inner}}\sqrt{2\pi}} \exp\left(\frac{-(m_{J/\psi K} - m_B)^2}{2\sigma_{\text{inner}}^2}\right), \quad (2)$$

$$\sigma_{\text{outer}} = c_0(1 + c_1 e^{-c_2 E_K}), \quad (3)$$

$$\sigma_{\text{inner}} = c_3 \sigma_{\text{outer}}. \quad (4)$$

The magnetic field of the DØ solenoid is not symmetric along the beam direction, but the reconstruction code uses a simplified symmetric field map. This results in small differences in reconstructed invariant masses between the  $\eta < 0$  and  $\eta > 0$  regions. To allow for these mass shifts a unique set of signal parameters is used for events in each of these regions.

The background PDF  $P(m_{J/\psi K}, E_K)$  describes  $B^\pm \rightarrow J/\psi \pi^\pm$  events in which the pion is misidentified as a kaon, resulting in an artificially high  $B^\pm$  mass. The PDF is a reflection of  $S$  with the mean shifted to recover the accurate pion mass and the widths shifted by a ratio of the means.

The background PDF  $T(m_{J/\psi K})$  describes all partially reconstructed  $B^\pm$  candidates. If a  $B^\pm$  decay has a final state with four or more particles, the reconstructed candidate will be missing a portion of its mass. These decays are modeled using a hyperbolic tangent function with an inflection point denoted  $t$ :

$$T(m_{J/\psi K}) = 1 - \tanh[25(m_{J/\psi K} - t)]. \quad (5)$$

Finally, the background PDF  $E(m_{J/\psi K}, E_K)$  describes the combinatorial background. It is modeled using an exponential function with a slope that depends on kaon energy:

$$E(m_{J/\psi K}, E_K) = e^{s(m_{J/\psi K} - 5.05)}, \quad (6)$$

$$s = s_0(1 + s_1 e^{-s_2 E_K}). \quad (7)$$

The unbinned fit minimizes the negative log of a likelihood function  $\mathcal{L}_n$  over  $N$  events, each with weight  $w_n$  (Sec. VI).  $\mathcal{L}_n$  is a function of the four PDFs described above. They are each assigned a sample fraction  $f_i$  and a forward-backward asymmetry  $A_i$ , which are all free parameters in the fit. The value of  $q_{FB}$  determines if a  $B^\pm$  candidate is forward or backward.  $\mathcal{L}_n$ , shown in Eq. 9, has 26 parameters and is normalized to 1.

$$\text{LLH} = -2 \sum_{n=1}^N w_n \ln(\mathcal{L}_n), \quad (8)$$

$$\begin{aligned} \mathcal{L}_n = & \alpha [f_S(1 + q_{FB}A_S)S(m_{J/\psi K}) + f_P(1 + q_{FB}A_P)P(m_{J/\psi K}) + f_T(1 + q_{FB}A_T)T(m_{J/\psi K})] \\ & + [1 - \alpha(f_S + f_P + f_T)](1 + q_{FB}A_E)E(m_{J/\psi K}), \end{aligned} \quad (9)$$

where  $\alpha$  describes the dependence of  $f_i$  on the energy,  $E_K$ , of the  $K^\pm$  [22].

## VI. CORRECTIONS FOR RECONSTRUCTION ASYMMETRIES

Asymmetries in  $J/\psi$  or  $K^\pm$  reconstruction between  $\eta < 0$  (the ‘‘south’’ half of the detector) and  $\eta > 0$  (the ‘‘north’’ half) can result in an apparent  $A_{FB}$ . Detector asymmetries have been measured from data samples with no expected production asymmetries. Decays of  $\phi \rightarrow K^+ K^-$  are used to measure the north-south asymmetry  $A_{NS}(K^\pm)$ . Events are selected in which two oppositely charged tracks form a vertex with a mass between 0.99 and 1.06 GeV/ $c^2$ . The tracks are selected using criteria which match the kinematic properties of the  $K^\pm$  candidates in the  $B^\pm \rightarrow J/\psi K^\pm$  sample. The kaon tracks must also have a minimum separation of  $\Delta\mathcal{R} = \sqrt{(\Delta\phi)^2 + (\Delta\eta)^2} > 0.15$ . The  $\phi \rightarrow K^+ K^-$  signal is modeled by a relativistic Breit-Wigner resonance convoluted with a double Gaussian resolution. Background

models are determined from Monte Carlo studies. A binned  $\chi^2$  minimization fit is performed simultaneously on north- and south-side data.  $A_{NS}(K^\pm)$  (Fig. 5(a)) is binned by the charge and  $|\eta|$  of the leading kaon; it does not show a significant dependence on  $p_T$ .

Prompt  $J/\psi \rightarrow \mu^+\mu^-$  decays are used to measure  $A_{NS}(J/\psi)$ . The selection criteria are those described in section IV, adding the requirement that the significance of the  $J/\psi$  decay length be less than 1.5, both to provide an orthogonal control sample and to ensure there are few  $B$  mesons in the sample. We estimate that only 2% of the sample is long-lived particles. Background events under the peak are removed with sideband subtraction, and  $A_{NS}(J/\psi)$  is calculated in bins of  $\eta$  and  $p_T$ , (Fig. 5(b)).

The main source of large  $A_{NS}(J/\psi)$  seen at low  $p_T$  appears to be detector asymmetries, specifically near the support structures at the base of the detector. A study of  $J/\psi$  occupancy shows that gaps in the region of the support structure are not symmetric about  $\eta = 0$ , and the response of the reconstruction algorithms to these gaps is momentum dependent (Fig. 6). The muon trigger system also contributes asymmetric effects which are time dependent. This time dependence is accounted for since the data samples used to determine the detector asymmetries are taken from the same dataset as the  $B^\pm$  signal events.

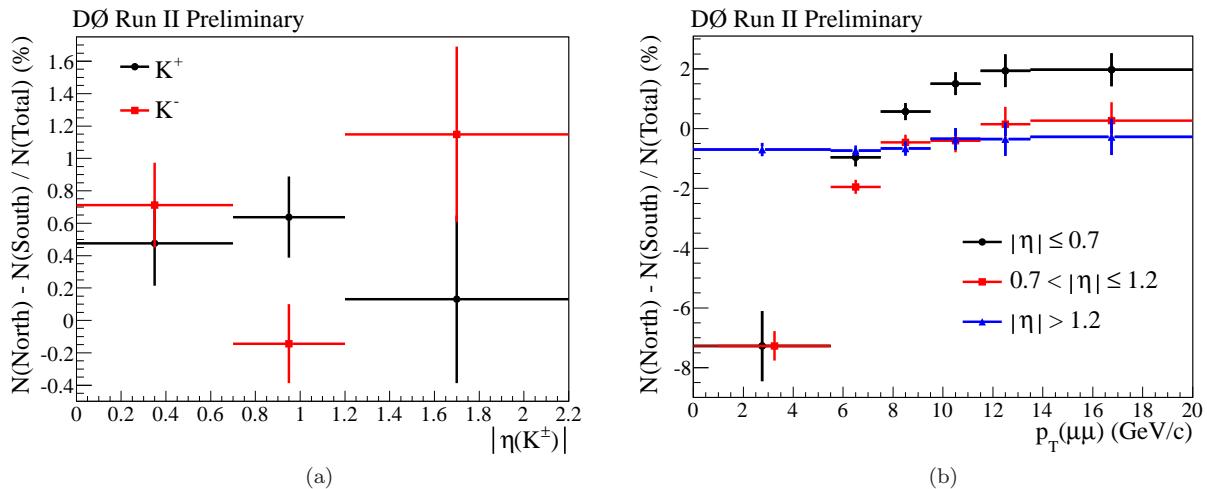


FIG. 5: Reconstruction asymmetries of (a)  $\phi \rightarrow K^+K^-$  decays in bins of leading kaon charge and  $|\eta|$  and (b) of prompt  $J/\psi \rightarrow \mu^+\mu^-$  decays in bins of  $|\eta|$  and  $p_T$ .

The  $A_{NS}$  values are used to equalize the relative reconstruction efficiencies on both sides of the detector. South-side particles are assigned efficiency  $\varepsilon_S = 1$ , and north-side particles are weighted so that  $\varepsilon_N = \varepsilon_S$ .

$$A_{NS} = \frac{\varepsilon_N - \varepsilon_S}{\varepsilon_N + \varepsilon_S}, \quad (10)$$

$$\varepsilon_S = \varepsilon_N \frac{1 - A_{NS}}{1 + A_{NS}}. \quad (11)$$

Since the background distributions could contain events without real  $J/\psi$  or  $K^\pm$  particles (e.g.,  $B^\pm \rightarrow J/\psi\pi^\pm$  events), the value of  $A_{NS}$  in the corrective weight is scaled by the expected signal fraction  $F$  of the event.

$$F(m_B, E_K) = \frac{\alpha f_S S}{\alpha(f_S S + f_P P + f_T T) + [1 - \alpha(f_S + f_P + f_T)]E}. \quad (12)$$

The overall weight for each event is  $w_n = w_{\text{magnet}} w_{J/\psi} w_{K^\pm}$ , where  $w_{\text{magnet}}$  equalizes the number of events in each setting of solenoid polarity, toroid polarity, and  $B^\pm$  charge. These weights are all nearly equal to unity due to regular magnet polarity reversal at DØ and the nearly equal numbers of  $B^+$  and  $B^-$  candidates. Equalizing the number of  $B^+$  and  $B^-$  candidates eliminates the need to correct for the different  $K^+$  and  $K^-$  cross sections with the detector material. The corrective weights  $w_{J/\psi}$  and  $w_{K^\pm}$  are:

$$w_X = \begin{cases} 1 & \text{for south-side } X = J/\psi, K^\pm \\ [1 - FA_{NS}(X)]/[1 + FA_{NS}(X)] & \text{for north-side } X = J/\psi, K^\pm \end{cases}. \quad (13)$$

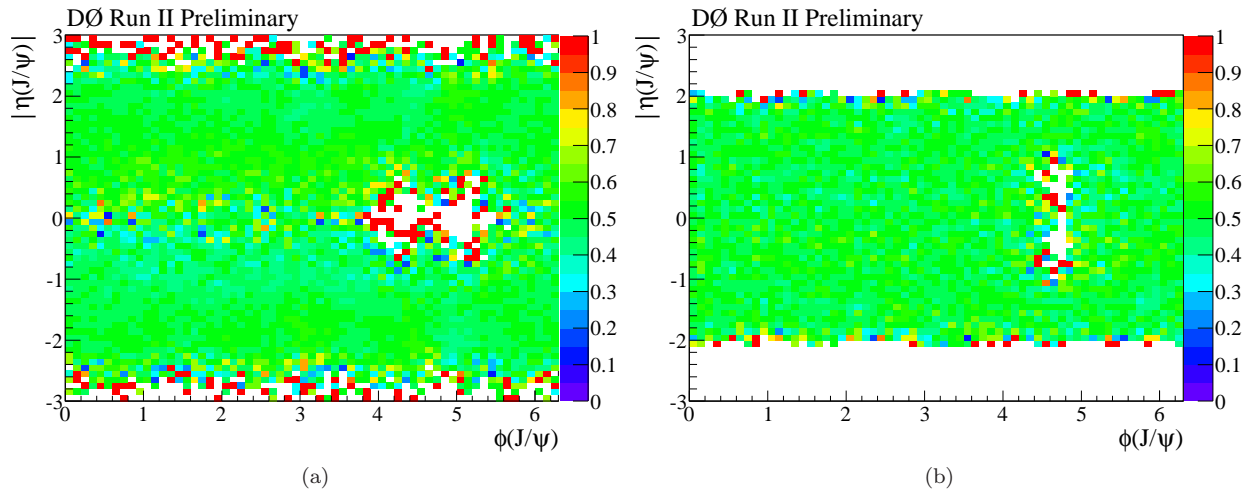


FIG. 6:  $J/\psi$  occupancy at (a) low transverse momentum ( $J/\psi$   $p_T < 5.5$  GeV/ $c$ ), and (b) high transverse momentum ( $J/\psi$   $p_T$  11.5 – 13.5 GeV/ $c$ ). Each bin of  $(\eta, \phi)$  is normalized by the number of events in the corresponding  $(|\eta|, \phi)$  bin. A value of 0.5 indicates that the events that bin are evenly distributed between the north and south sides, while values near 0 or 1 reflect a large  $A_{NS}$ .

The values of  $A_{NS}$  are determined by the kinematic bins of the  $J/\psi$  and  $K^\pm$ .

Applying these reconstruction asymmetry weights has an effect on  $A_{FB}(B^\pm)$ , labeled  $A_{FB}(\text{corr})$ , which is calculated by comparing uncorrected fits to weighted fits:  $A_{FB}(\text{corr}) = A_{FB}(\text{uncorrected}) - A_{FB}(\text{weighted})$ . The event-by-event weighting method is cross-checked using a weighted average of  $A_{NS}(J/\psi)$  and  $A_{NS}(K^\pm)$  over their kinematic bins [23], with the number of signal events per bin extracted from binned fits of the  $B^\pm \rightarrow J/\psi K^\pm$  data. These two methods of calculating  $A_{FB}(\text{corr})$  are consistent.

## VII. FIT RESULTS

In the initial stages of this analysis, the value of  $A_{FB}$  was blinded, either with an event-by-event randomization of  $q_{FB}$  or with an unknown random offset to the value of  $A_{FB}$ . Before unblinding, a set of 1000 pseudo-experiments, each with  $q_{FB}$  blinded based on a new random seed, was used to confirm the statistical uncertainty of the fit (Fig. 7(a)). There is an additional statistical uncertainty of 0.002% due to the uncertainties on  $A_{NS}(J/\psi, K^\pm)$  which form the corrective weights. This uncertainty is determined using 500 pseudo-experiments with Gaussian variations of the  $A_{NS}$  values (Fig. 7(b)). For each trial each of the corrective weights is randomized with a Gaussian distribution, with a width determined by its error. The fit method was calibrated by injecting a series of fifty test asymmetries to the blinded data. The test was repeated with five sets of fifty random seeds to blind  $q_{FB}$ . Figure 8 shows that the fit succeeds in returning the input asymmetry values.

After numerous systematic checks, the fits were unblinded. The  $B^\pm \rightarrow J/\psi K^\pm$  final fit, corrected for reconstruction asymmetries, gives  $88664 \pm 517$  signal events. The projection of the unbinned fit onto the (forward + backward) invariant mass distribution is shown in Fig. 9. The fitted PDFs multiplied by their associated asymmetry parameters are projected onto the (forward – backward) mass distribution (Fig. 10), where each data event is given a positive or negative weight according to  $q_{FB}$ .

Although the fit is unbinned, fit quality is estimated by creating distributions of residuals, shown in Fig. 11. The quadrature sum of these residuals is taken as the  $\chi^2$  value for the distribution. The full fit has 26 free parameters, 22 of which we consider constrained by the (forward + backward) distribution. This distribution has 120 bins and 98 degrees of freedom, for a  $\chi^2/\text{ndf}$  of 1.27. The residuals of the (forward – backward) distribution are shown in Fig. 11(b). If we consider the 4 asymmetry parameters to be constrained by this distribution it has 116 degrees of freedom, for a  $\chi^2/\text{ndf}$  of 0.96.

The fully corrected, unblinded fit gives a signal asymmetry consistent with zero.

$$A_{FB}(B^\pm) = [-0.26 \pm 0.41 (\text{stat.})].\% \quad (14)$$

The background asymmetries are also consistent with zero:  $A_P = (0.57 \pm 11.67)\%$ ,  $A_T = (-2.02 \pm 3.58)\%$ , and  $A_E = (0.44 \pm 0.74)\%$ .

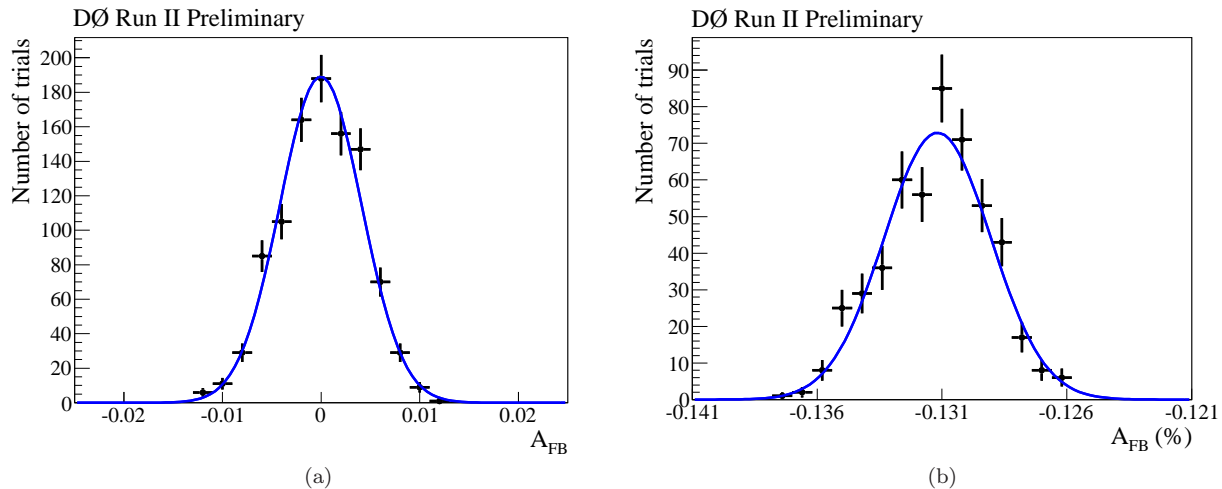


FIG. 7: (a)  $A_{FB}(B^\pm)$  values from 1000 pseudoexperiments randomizing the sign of  $\eta_B$ . The mean value of all pseudoexperiments is zero as expected, and the width of  $0.42 \pm 0.01$  is consistent with the statistical uncertainty of 0.41% returned by the fit. (b) 500 Gaussian randomizations of the  $A_{NS}$  corrective weights. Each trial uses the same random seed for the  $\eta_B$  blinding, giving a mean value of -0.13%. The width of this distribution gives the statistical uncertainty of 0.002% from the corrective weighting procedure.

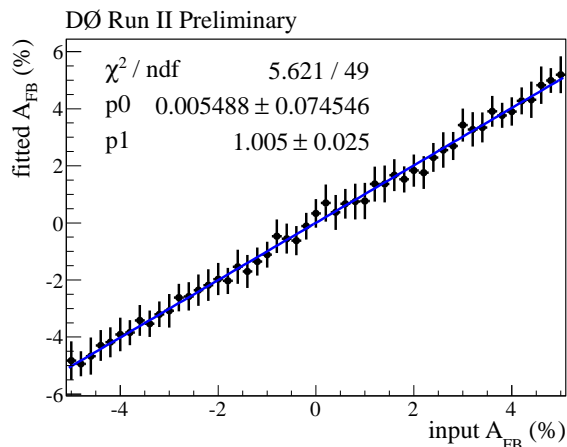


FIG. 8: Fitted values of  $A_{FB}$  versus the input values, in data with  $q_{FB}$  randomized. The data points combine five sets of fits with unique random seeds for each input asymmetry. The best fit line has an offset consistent with zero and a slope consistent with one, which shows the fit measures the expected asymmetries.

## VIII. SYSTEMATIC UNCERTAINTIES

To determine systematic uncertainties numerous reasonable variations are made to the fitting method. Two alternative BDTs were considered, one with the minimum  $M(J/\psi K)$  of the lower background sideband increased to 4.5 GeV/ $c^2$  to improve agreement of the background distributions with the background in the analysis range. A second alternative was trained without isolation variables to test any bias against high momentum  $B$  mesons.

The mass range for the  $B^\pm$  candidates in the fit is varied by 50 MeV/ $c^2$  in 10 MeV/ $c^2$  steps, on both edges (30 variations). The kaon energy dependences in the PDFs ( $\sigma_{\text{outer}}$ ,  $s$ , and  $\alpha$ ) are removed in all possible combinations (7 variations). The partial reconstruction PDF has a fixed slope parameter which can be allowed to float, while the inflection point parameter either floats or is fixed (3 variations). The background asymmetry parameters are fixed to zero, or  $A_T$  is set equal to  $A_E$  (6 variations). Finally, the number of events in each magnet weight setting is increased or decreased by its statistical error  $\sqrt{N}$  (16 variations).

Multiple data samples were considered for deriving the reconstruction asymmetries.  $A_{NS}(J/\psi)$  could be replaced with  $A_{NS}$  calculated for the individual muons, and  $A_{NS}(K^\pm)$  could be replaced with  $A_{NS}$  calculated from a sample

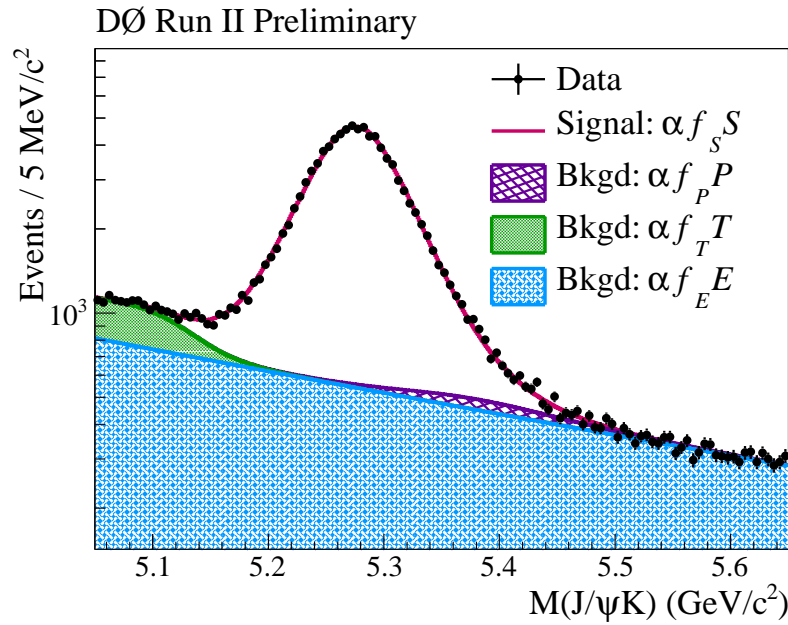


FIG. 9:  $B^\pm \rightarrow J/\psi K^\pm$  invariant mass distribution of the final data sample with fitted PDF curves.

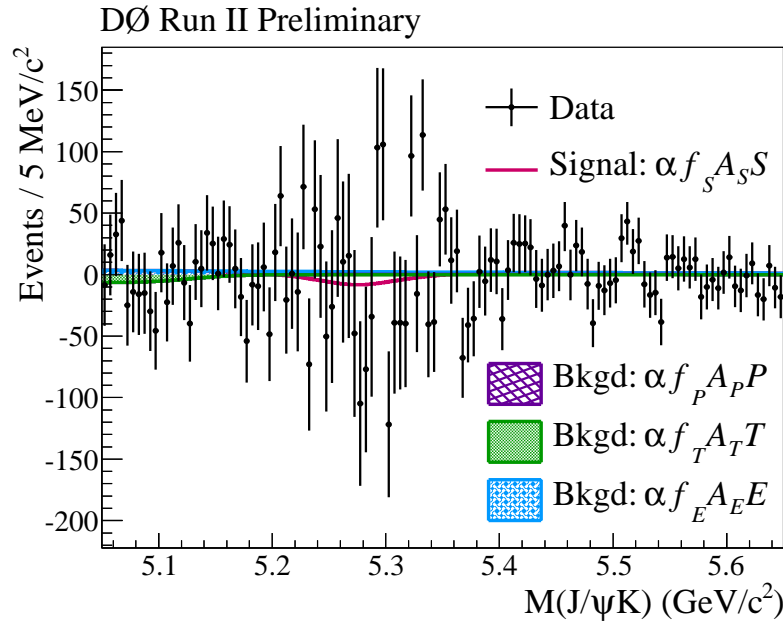


FIG. 10: (Forward – backward) invariant mass distribution. The fitted PDFs are multiplied by the corresponding asymmetry parameters.

of random charged tracks. These samples were rejected for degrading the agreement between  $A_{FB}(B^+)$ ,  $A_{FB}(B^-)$ , and  $A_{FB}(B^\pm)$ . The calculations of  $A_{NS}(J/\psi, K^\pm)$  each have three versions, representing different selection cuts, binning, or fit parameters.

The calibration of the fit, shown in Fig. 8, reveals small biases and non-linearities in the fit method. For the observed  $A_{FB}(B^\pm)$  of  $-0.26\%$ , the calibration line indicates a true asymmetry of  $-0.264\%$ . The shift of  $0.004\%$  is negligible based on the precision of our measurement, so it is added as a systematic uncertainty.

For sets of less than eight variations, the uncertainty is assigned to be half the largest variation in the central value. For larger sets the uncertainty is one standard deviation:  $\sigma = \sqrt{(x - \bar{x})^2/N}$ . These variations give a total uncertainty of  $0.01\%$  and are summarized in Tab. I.

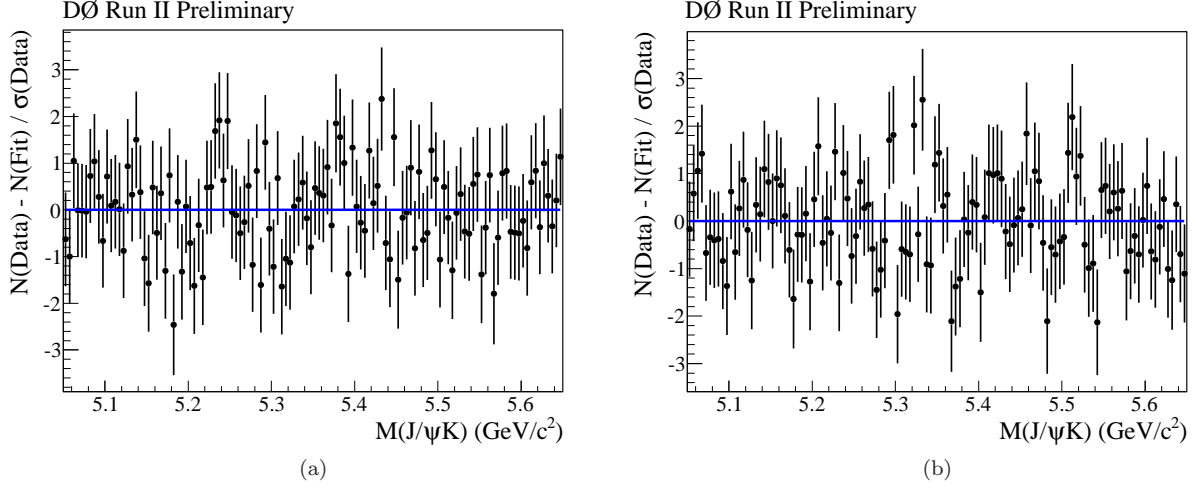


FIG. 11:  $[N(\text{data}) - N(\text{fit})]/\sigma_{N(\text{data})}$  for each bin of the (a) F + B and (b) F - B mass distributions. The even distribution about zero reflects the lack of bias in the fits.

TABLE I: Summary and Combination of Uncertainties

Source	Uncertainty
Statistical (Fit + $A_{NS}$ Weighting)	0.41%
Alternative BDTs (min. $M(J/\psi K) = 4.5 \text{ GeV}/c^2$ ; no isolation variables)	0.14%
Mass Range Extensions (up to 50 MeV extensions of both edges)	0.01%
Fit Function ( $E_K$ dependences on/off + fix/float $T$ slope and inflection)	0.04%
Background Asymmetry Modeling (float/fix $A_P, A_E, A_T$ parameters)	0.07%
Magnet Weighting (vary each of 8 subsamples by $\pm\sqrt{N}$ )	0.0001%
Reconstruction Asymmetries (alternate samples + calculation revisions)	0.06%
Fit Calibration (input asymmetry test, Fig. 8)	0.004%
Systematic Uncertainty	0.17%
Total Uncertainty	0.44%

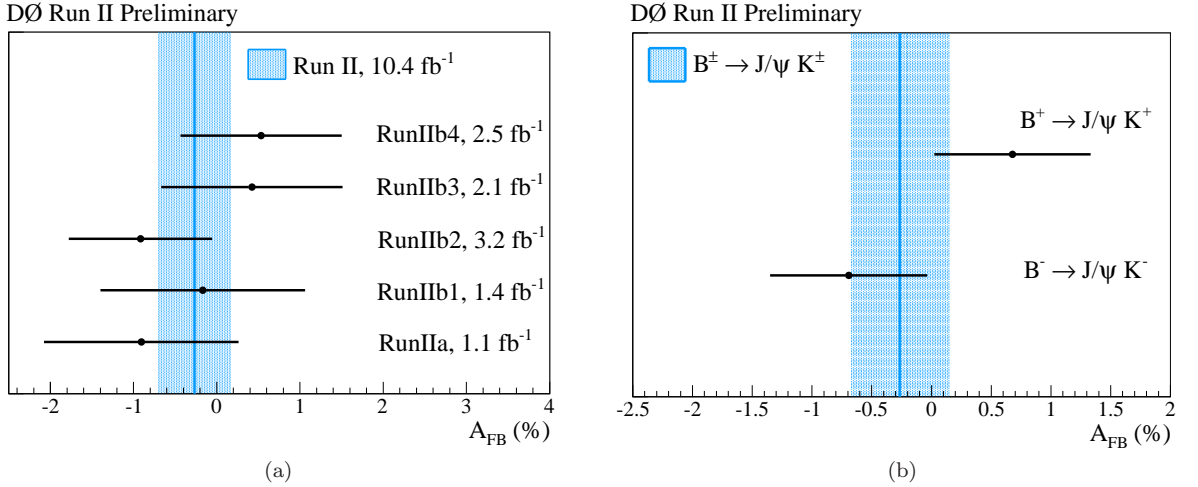


FIG. 12: Stability of  $A_{FB}(B^\pm)$  in different (a) Run II data epochs and (b)  $q_B$  settings. Errors on split samples are statistical only; the full sample shows the total uncertainty.

## IX. STABILITY TESTS AND BINNED MEASUREMENTS

The stability of the asymmetry measurement can be tested by dividing the data into subsets. Figure 12 shows the consistency of the measurement over time and with  $B^+$  and  $B^-$  samples fitted separately. Separate signal parameters for the north and south sides of the detector were required to bring these values into agreement before unblinding the data. Figure 13 shows that the measurement of  $A_{FB}(B^\pm)$  in data is stable across the range of momenta and pseudorapidity.

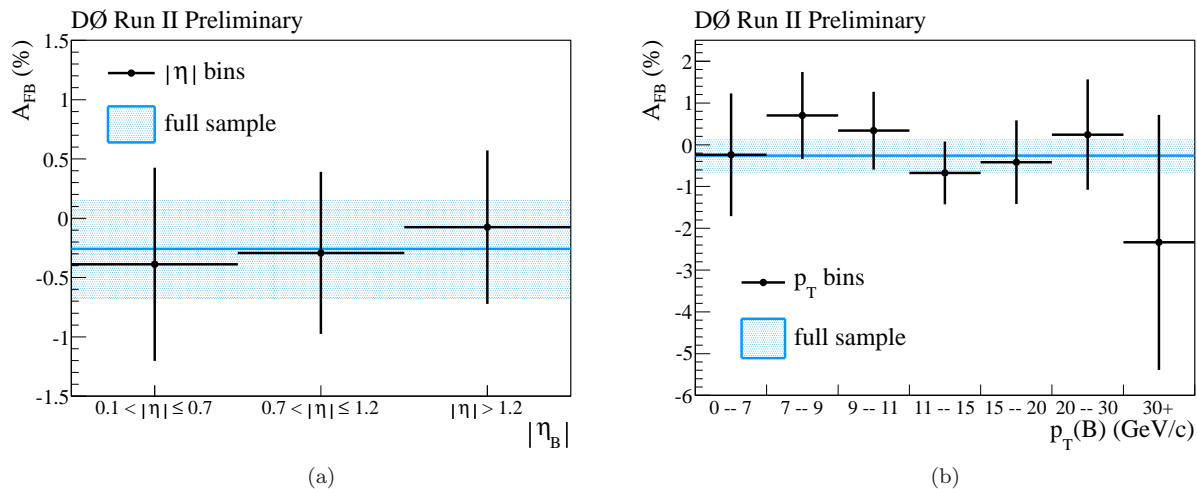


FIG. 13:  $A_{FB}(B^\pm)$  in bins of (a)  $|\eta_B|$  and (b)  $p_T(B)$ . Errors on split samples are statistical only; the full sample shows the total uncertainty.

## X. CONCLUSIONS

The forward-backward asymmetry in  $B^\pm \rightarrow J/\psi K^\pm$  decays is measured using a maximum log likelihood fit. The asymmetry  $A_{FB}(B^\pm)$  is shown to be stable over a diverse range of subsets of the data. The preliminary result for the inclusive data sample is  $A_{FB}(B^\pm) = [-0.26 \pm 0.41 \text{ (stat.)} \pm 0.17 \text{ (syst.)}]%$ , which is the first measurement of this quantity. Standard model predictions from MC@NLO are in preparation.

## XI. ACKNOWLEDGEMENTS

We thank the stas at Fermilab and collaborating institutions, and acknowledge support from the DOE and NSF (USA); CEA and CNRS/IN2P3 (France); MON, NRC KI and RFBR (Russia); CNPq, FAPERJ, FAPESP and FUNDUNESP (Brazil); DAE and DST (India); Colciencias (Colombia); CONACyT (Mexico); NRF (Korea); FOM (The Netherlands); STFC and the Royal Society (United Kingdom); MSMT and GACR (Czech Republic); BMBF and DFG (Germany); SFI (Ireland); The Swedish Research Council (Sweden); and CAS and CNSF (China).

- 
- [1] J.H. Kühn and G. Rodrigo, Phys. Rev. D **59**, 054017 (1999).
  - [2] L.G. Almeida, G. Sterman, and W. Vogelsang, Phys. Rev. D **78**, 014008 (2008); J.H. Kühn and G. Rodrigo, J. High Energy Phys. 01 (2012) 063.
  - [3] V.M. Abazov *et al.* (D0 Collaboration), Phys. Rev. D **84**, 112005 (2011);
  - [4] T. Aaltonen *et al.* (CDF Collaboration), Phys. Rev. D **88**, 072003 (2013); T. Aaltonen *et al.* (CDF Collaboration), Phys. Rev. D **87**, 092002 (2013); T. Aaltonen *et al.* (CDF Collaboration), Phys. Rev. D **83**, 112003 (2011);
  - [5] V. M Abazov *et al.* (D0 Collaboration), arXiv:1405.0421 (2014) (submitted to Phys. Rev. D); V. M Abazov *et al.* (D0 Collaboration), arXiv:11403.1294 (submitted to Phys. Rev. D); V. M Abazov *et al.* (D0 Collaboration), Phys. Rev. D **88**, 112002 (2013); V. M Abazov *et al.* (D0 Collaboration), Phys. Rev. D **87**, 011103 (R) (2013);

- [6] S. Chatrchyan *et al.* (CMS Collaboration), *J. High Energy Phys.* 04 (2014) 191.
- [7] G. Aad *et al.* (Atlas Collaboration), *J. High Energy Phys.* 02 (2014) 107.
- [8] B. Grinstein and C.W. Murphy, *Phys. Rev. Lett.* **111**, 062003 (2013).
- [9] R. Aaij *et al.* (LHCb Collaboration), arXiv:1406.4789 (2014).
- [10] CDF Collaboration, CDF/ANAL/TOP/PUB/11092 (2014).
- [11] V.M. Abazov *et al.* (D0 Collaboration), *Nucl. Instrum. Methods A* **565**, 463 (2006).
- [12] R. Angstat *et al.* (D0 Collaboration), *Nucl. Instrum. Methods A* **622**, 298 (2010).
- [13] A.V. Manohar and M. Trott, *Phys. Lett. B* **711**, 313 (2012).
- [14] S. Frixione and B.R. Webber, *J. High Energy Phys.* 06 (2002) 029; S. Frixione, P. Nason, and B.R. Webber, *J. High Energy Phys.* 08 (2003) 007.
- [15] P.M. Nadolsky *et al.*, *Phys. Rev. D* **78**, 013004 (2008).
- [16] G. Corcella, *J. High Energy Phys.* 01 (2001) 010.
- [17] R. Brun and F. Ceminri, CERN Program Library W5013, 1993. We use GEANT version 3.15.
- [18] V.M. Abazov *et al.* (D0 Collaboration), *Nucl. Instrum. Methods A* **737**, 281 (2014).
- [19] J. Beringer *et al.*, *Phys. Rev. D* **86**, 010001 (2012).
- [20] A. Hoecker *et al.*, “Toolkit for Multivariate Data Analysis”, arXiv:physics/0703039v5 (2007). We use version 4.1.0.
- [21] T. Sjöstrand, S. Mrenna, and P. Skands, *J. High Energy Phys.* 05 (2006) 026.
- [22] V.M. Abazov *et al.* (D0 Collaboration), *Phys. Rev. Lett.* **110**, 241801 (2013).
- [23] V.M. Abazov *et al.* (D0 Collaboration), *Phys. Rev. D* **86**, 072009 (2012).